Supplementary Material

The hierarchical porosity of three-dimensional graphene electrode for binder-free and high performance supercapacitors

Jun-He Chang , Yu-Han Hung, Xu-Feng Luo,Chi-Hsien Huang, Sungmi Jung, Jeng-Kuei Chang, Jing Kong and Ching-Yuan Su *

Figure S1 (a)The HRTEM image for the sample without activation treatment. It is clear seen that the even in magnified image in (b) there is no apparent porous structure been observed on the flake surface. In the other hand, (c) and (d) are the HRTEM images for the porous graphene by acid activation. The nanopore size distribution of the activated graphene by statistical study from HRTEM image. (d) shows the magnified TEM image where the red lines indicate the estimated diameter for the holes, here 21 randomly selective pores were calculated. (e)The distributed nanopores size in (d) shows that the mainly pores size are narrowed at 2.5~2.8 nm in diameter.

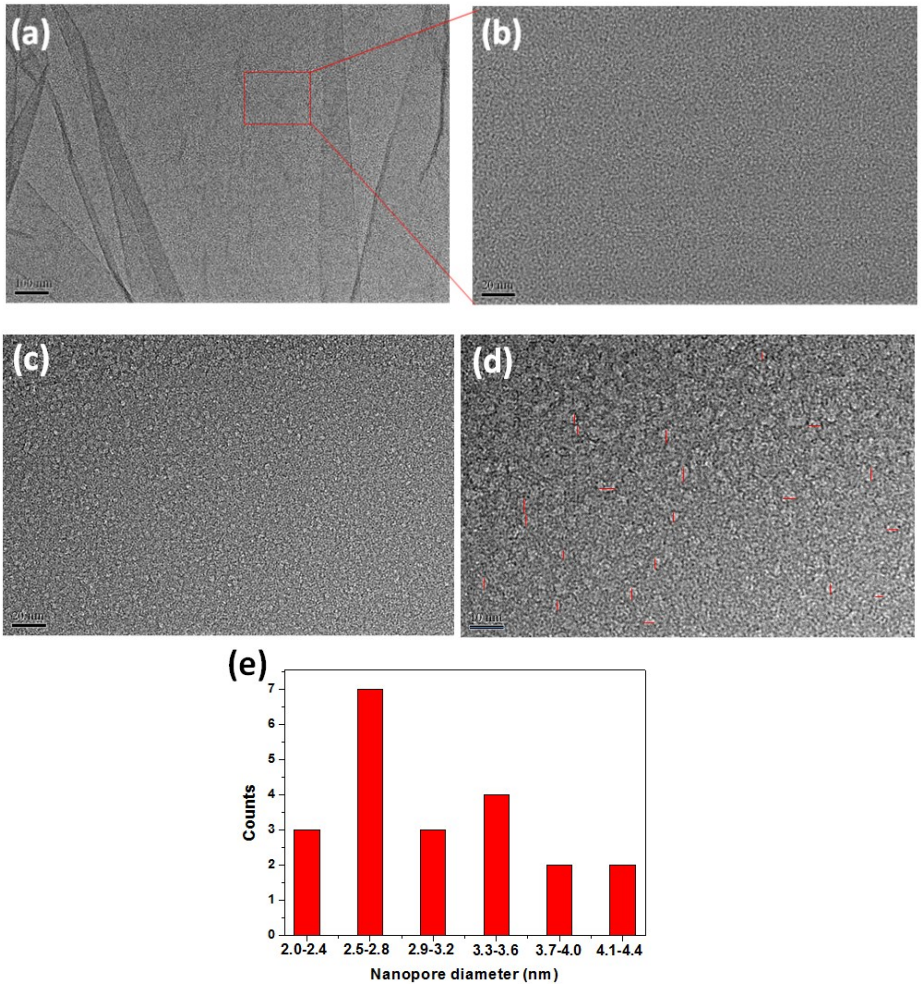

Figure S2. The illustration (a) and photoimage(b) for the three-electrodes testing setup. (c) The photo image of the sample when the electrode was subjected to 2000 cycling test. There were no apparent phenomenon of peel –off graphene from electrode, suggesting the mechanical strength and operational reliable of as-prepared 3D porosity graphene electrode .

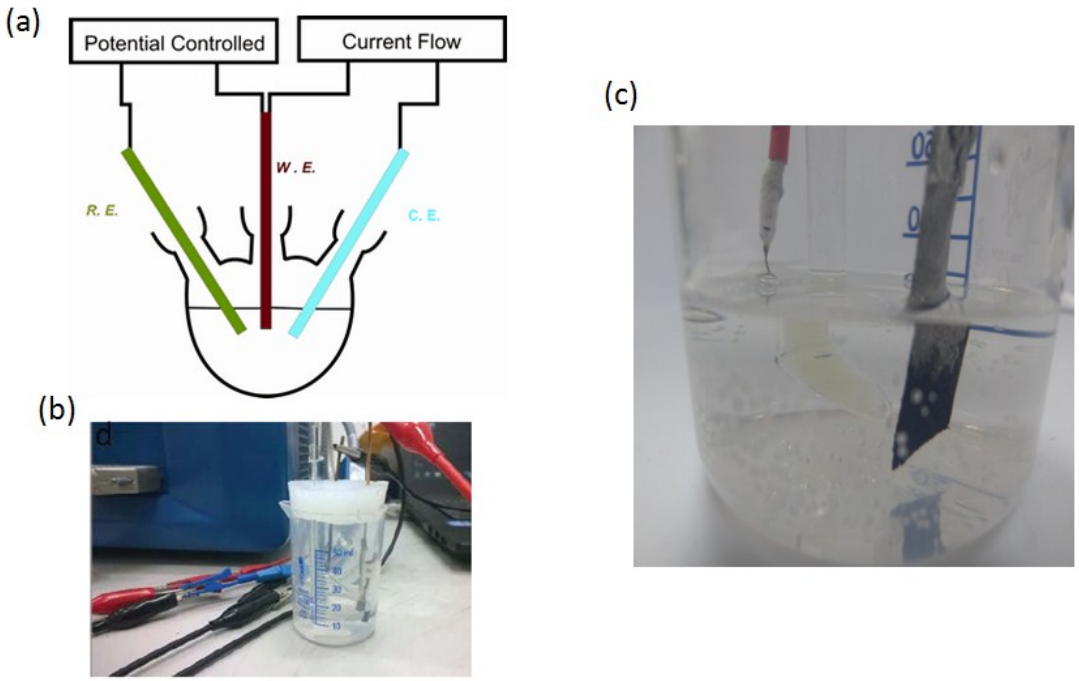

Figure S3. The comparison of morphology for (a) pristine Ni foam and graphene electrodes: (b)The crumpling and restacking rGO on Ni ligaments when the sample were prepared by the thermal drying method. (c) The porous 3D graphene interconnected over the Ni foam electrode by freeze-drying approach.

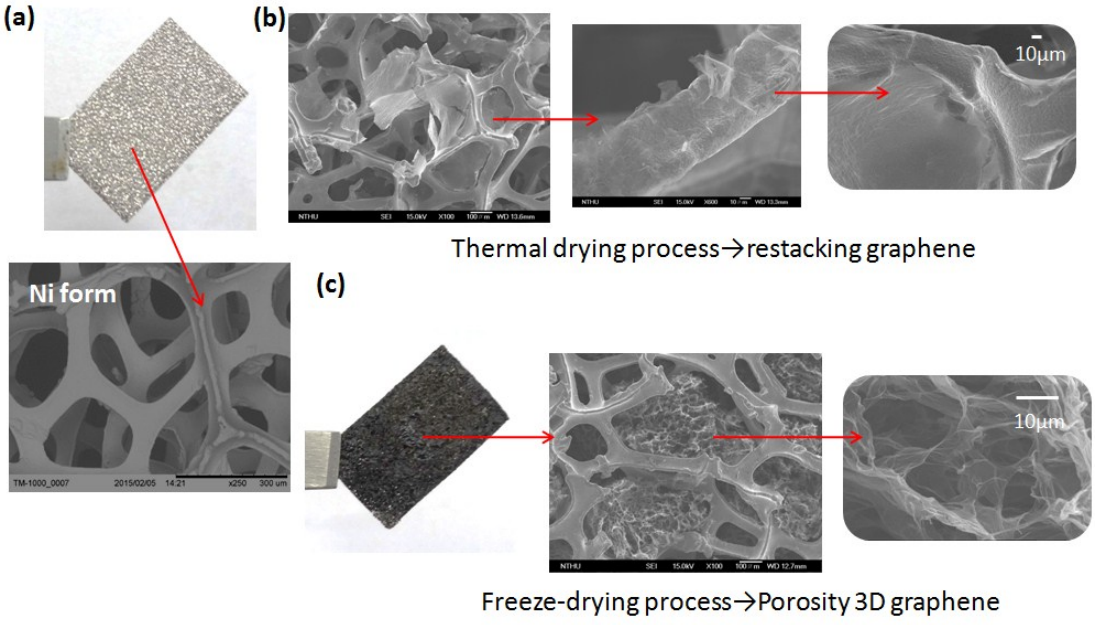

Figure S4. (a) The C-V curve shows the less capacitance contribution from the supporting electrode of Ni foam when it was compared to that samples with Ni foam supported graphene electrode. (b) The cycling testing shows no much variations after three cycles.

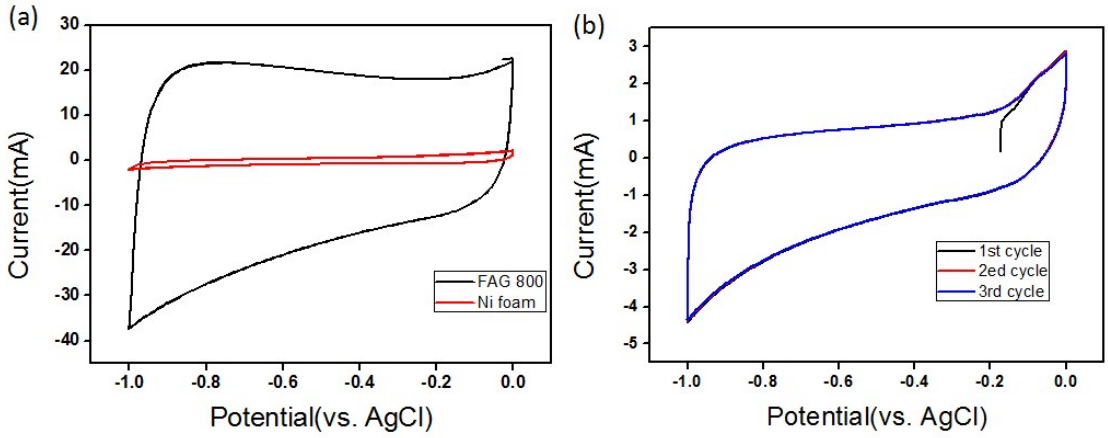

Figure S5 The CV curves with various scan rate for the conditions of (a)AG400 ,(b)AG600, (c)AG800, (d)FAG400 ,(e)FAG600 and (f) FAG 800.

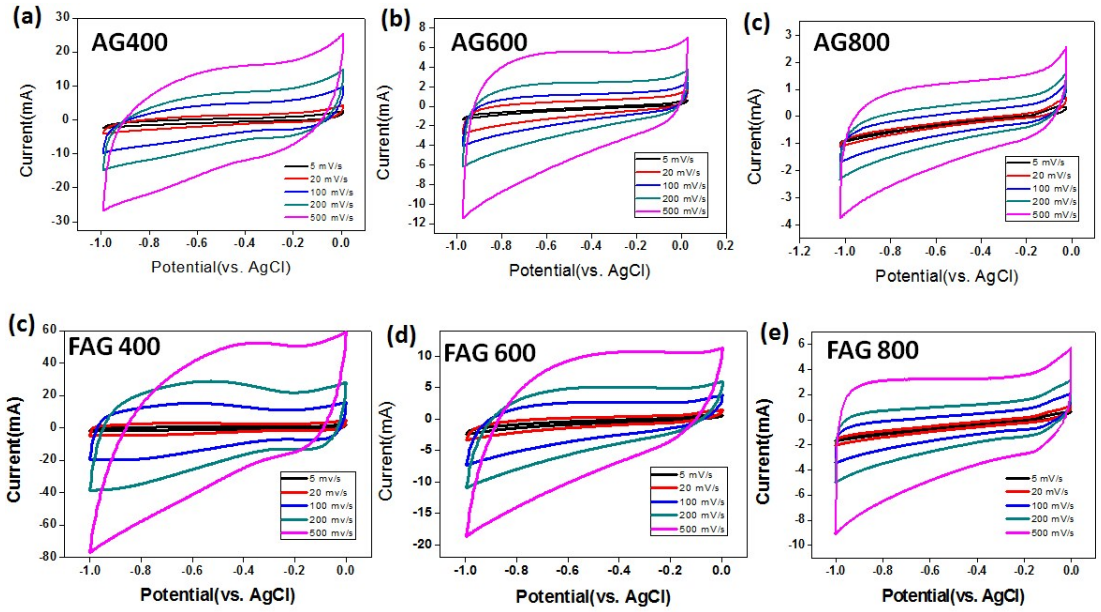

Figure S6. (a)The water contact angle measurement for three annealed sample at various temperatures where the measured angles are 73°(G400), 87°(G600), and 88°(G800). (b) The electrical resistance for three samples. (c) The typical CV curves for the three samples. Although the electrical conductivity for 400°C annealing is much lower than the other two samples, the enhanced electrolyte wettibility on graphene surface could dominate the electrochemical performance of the graphene electrode.

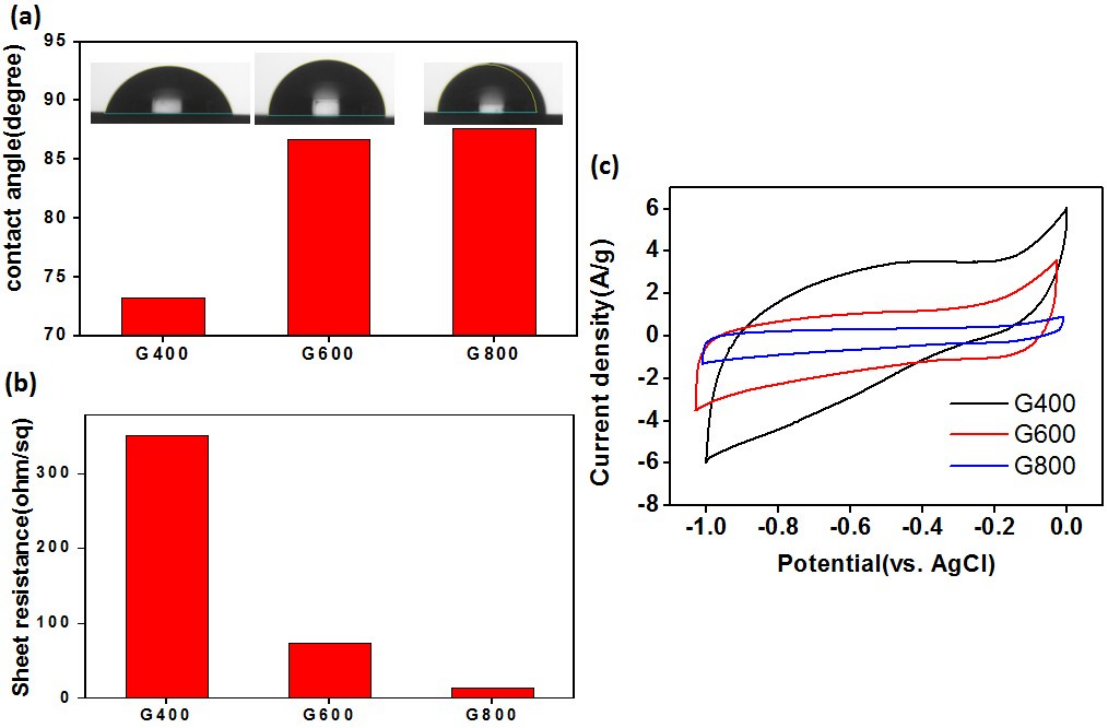

Figure S7 The detail study on the optimized conditions for the graphene electrodes of thermal reduction at 300°C (FAG300) and 500°C(FAG 500).

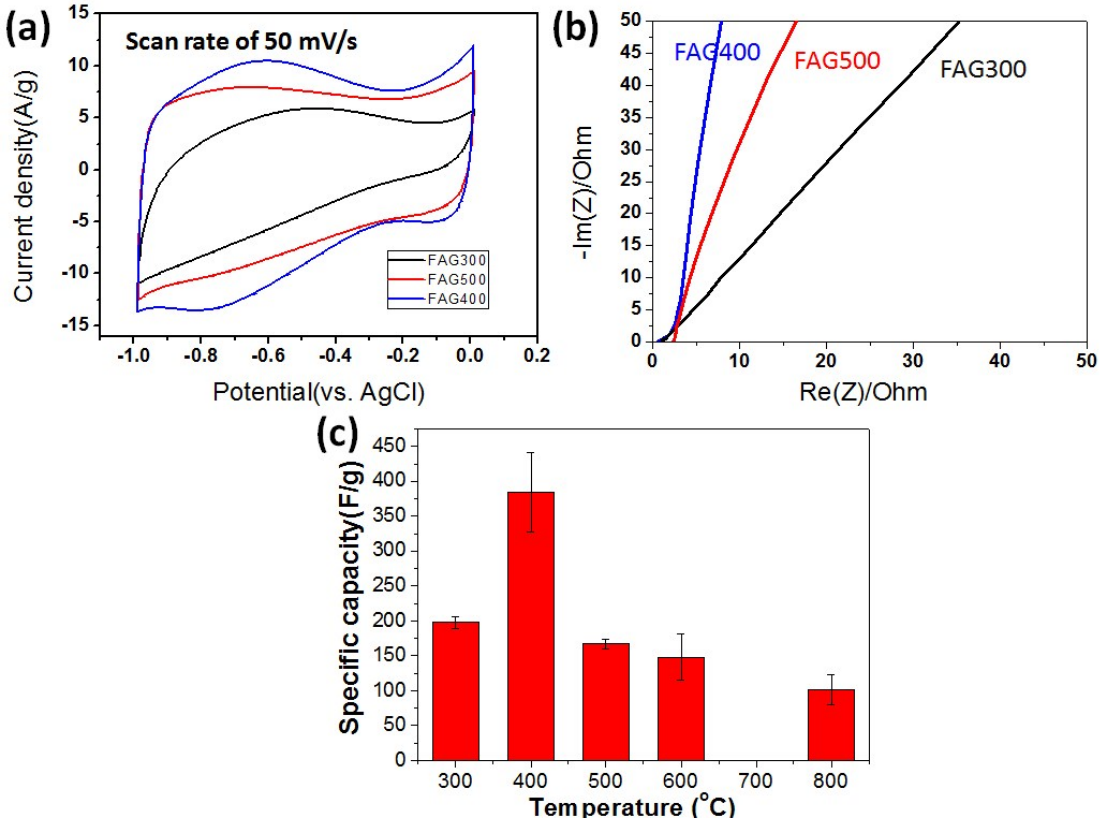

Figure S8 The correlation between the scan rate (in CV test) and current density(in rate capacitance). The rate capacitance as shown in Fig 5d is lower than the obtained capacitance in CV test due to the different scan rate. For example, the current density of 2A/g in rate capacitance curve for FAG400 is corresponding to the scan rate of 8 mV/s, which is higher than that in CV test(5 mV/s)

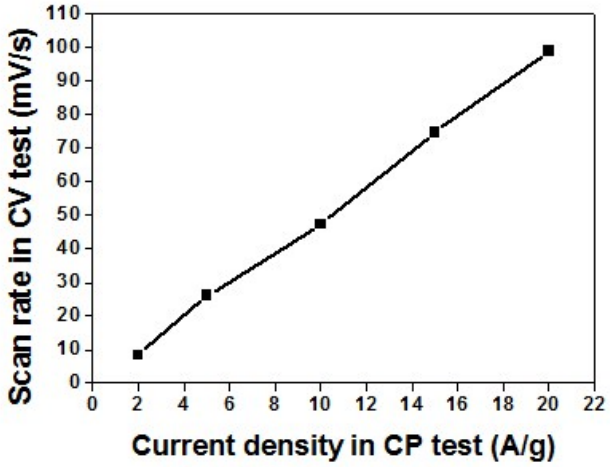

Table S1 The performance comparisons of this work with these reported graphene-supercapacitors.

Ref.	Preparation Method and structures	Electrolyte	Specific Capacitance (F/g)[(a)]
This work	The hierarchical 3D porosity of graphene electrode	KOH	384
[1]	Stacking graphene electrode by hydrazine reduction	KOH	135
		TEABF4	99
[2]	Stacking graphene electrode by hydrothermal reduction	KOH	175
[3]	Stacking graphene electrode by Solvothermal reduction	Na_2SO_4	218
[4]	Active graphene by KOH	(BMIM BF4)/AN	166
[5]	Active graphene by H_2O_2-etched	KOH	310
[6]	3D porosity of graphene electrode	H_2SO_4	325
[7]	3D graphene- aerogel-based mesoporous carbons	H_2SO_4	226
[8]	3D marcoporous graphene films	H_2SO_4	173
[9]	Crumpled N-doped graphene	KOH	248
[10]	B, N Co-doped graphene	H_2SO_4	239
[11]	Mesoporous graphene with 3D structure	KOH	341
[12]	Holey graphene framework	KOH	298

Figure S9 Summary of Ragone plots of this work compared to previous studies on supercapacitors with 3D graphene electrodes.

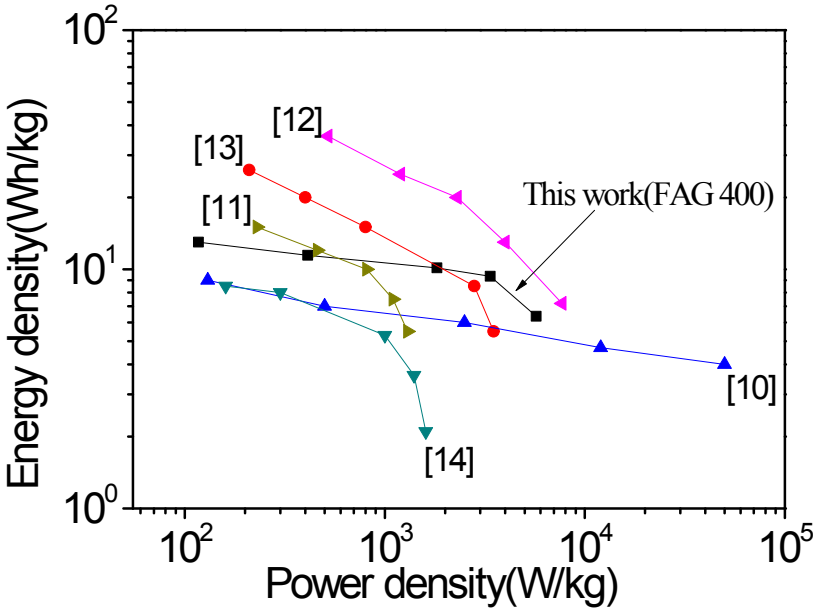

Figure S10. The Ragone plot of power density versus energy density for symmetric supercapacitors with different graphene electrodes in this study.

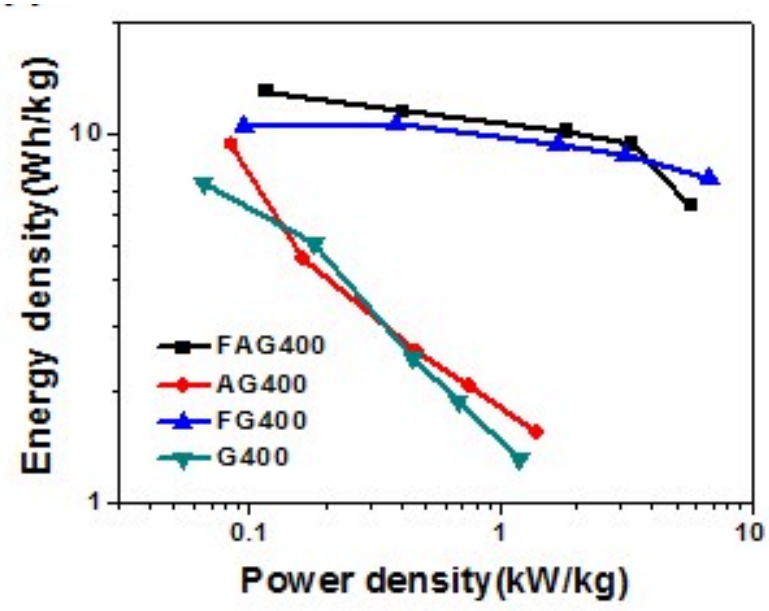

Figure S11. The Brunauer–Ennett–Teller (BET) characterization for the sample FAG 400. (a) N_2 adsorption–desorption isotherms of FAG 400 with ~27.3 m^2/g. (b) The pore volume and pore size destitution.

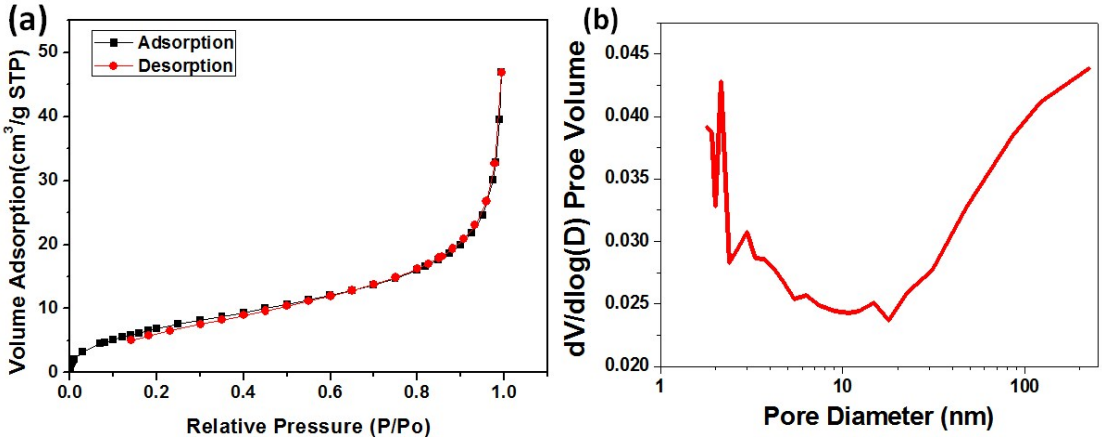

Reference:

[1] Stoller, M. D., et.al., **Nano Lett.** 2008 , 8 , 3498

[2] Xu , Y. et.al., **ACS Nano** 2010 , 4 , 4324 .

[3] Lai,L. F., et.al., **Carbon** 2011 , 49 , 3250 .

[4] Zhu,Y., et.al., **Science** 2011, 332, 1537.

[5] Xu, Y., et al., **Nat. Commun.** , 2014. 5: p. 4554.

[6] Jung, S. M., et.al., **Nanoscale**, 2015, 7, 4386.

[7] Wu, Z. S., et al., **J. Am. Chem. Soc**., 2012. 134(48): p. 19532.

[8] Lee, S.H., et al., **An. Chem. Inter. Edi.,** 2010. 49(52): p. 10084.

[9] Wen, Z., et al., **Adv.Mat.**, 2012. 24(41): p. 5610.

[10] Wu, Z.-S., et al., **Adv.Mat.**, 2012. 24(37): p. 5130.

[11] Hu, J., et al., **Carbon**, 2014. 67: p. 221.

[12] Xu, Y., et al., **Nat Commun.** , 2014. 5: p. 4554.

[13] Lee, J.H., et al., **ACS Nano**, 2013. 7(10): p. 9366.

[14] Wang, X., et al., **Nat Commun**, 2013. 4: p. 2905.